Camilla Mathison[1,2], Eleanor Burke[1], Andrew Hartley[1], Douglas I Kelley[4], Eddy Robertson[1], Chantelle Burton[1], Nic Gedney[1], Karina Williams[1,3], Andy Wiltshire[1,3], Richard J Ellis[4], Alistair A Sellar[1], Chris D. Jones [1]

[1] Met Office Hadley Centre, FitzRoy Road, Exeter, UK

[2] School of Earth and Environment, Institute for Climate and Atmospheric Science, University of Leeds, Leeds, UK

[3] Global Systems Institute, University of Exeter, Laver Building, North Park Road, Exeter, UK

[4] UK Centre for Ecology and Hydrology, Wallingford, Oxfordshire, OX10 8BB, UK

Corresponding author: Andrew Hartley (andrew.hartley@metoffice.gov.uk)

Key Points

- New land surface modelling capability applied to inter-sectoral impacts model inter-comparison
- We describe and evaluate the setup with and without fire against historical observations of relevance to large scale climate impacts

Abstract

Global studies of climate change impacts that use future climate model projections also require projections of land surface changes. Simulated land surface performance in Earth System models is often affected by the atmospheric models' climate biases, leading to errors in land surface projections. Here we run the JULES-ES land surface model with ISIMIP2b bias-corrected climate model data from 4 global climate models (GCMs). The bias correction reduces the impact of the climate biases present in individual models. We evaluate JULES-ES performance against present-day observations to demonstrate its usefulness for providing required information for impacts such as fire and river flow. We simulate a historical and two future scenarios; a mitigation scenario RCP2.6 and RCP6.0, which has very little mitigation. We include a standard JULES-ES configuration without fire as a contribution to ISIMIP2b and JULES-ES with fire as a potential future development. Simulations for gross primary productivity (GPP), evapotranspiration (ET) and albedo compare well against observations. Including fire improves the simulations, especially for ET and albedo and vegetation distribution, with some degradation in shrub cover and river flow. This configuration represents some of the most current earth system science for land surface modelling. The suite associated with this configuration provides a basis for past and future phases of ISIMIP, providing a simulation setup, post-processing and initial evaluation using ILAMB. This suite ensures that it is as straightforward, reproducible and transparent as possible to follow the protocols and participate fully in ISIMIP using JULES.

Plain Language Summary

This paper is significant because it describes and evaluates a new modelling methodology that can be used in future to quantify the impacts of climate change on water, biomes and the carbon cycle. We have created a new configuration and setup for the JULES-ES land surface model. We drive JULES-ES with bias-corrected historical and future climate model output provided by the Inter-Sectoral Impacts Model Inter-comparison Project (ISIMIP), allowing us to compare projections of the impacts of climate change across multiple impacts models. We evaluate the setups' simulated river flow, atmospheric fluxes of moisture, carbon and radiation, global biomes and fire against long-term climate data records. Including fire in the model was found to improve the distribution of biomes, which we recommend for future versions of this configuration. We have made the setup and outputs openly available. As we used the ISIMIP standard modelling protocol, other researchers can compare impact projections from climate change alongside impacts models taking part in ISIMIP.

Introduction

The Joint UK Land Environment Simulator (JULES) (Best et al., 2011; Clark et al., 2011) is a community-supported and developed land surface model used by land, hydrological, weather and climate communities. JULES is a configurable code base supporting weather, climate and earth system science applications. Here, we describe and evaluate the JULES Earth System (JULES-ES) configuration and experimental setup used in the Inter-Sectoral Impact Model Intercomparison Project (ISIMIP; Frieler et al., 2017). JULES-ES builds on the JULES-GL7 configuration described in Wiltshire et al. (2020) by including processes necessary for representing impacts and terrestrial biogeochemical processes. Whilst we run JULES-ES in offline mode, it is also coupled to the atmosphere within the earth system model UKESM (Sellar et al., 2019). Climate change impacts are already a feature of everyday life for much of the world, and quantifying these allows us to understand future benefits and trade-offs of climate mitigation and adaptation policies. ISIMIP provides a consistent framework for assessing impacts using a large ensemble of impacts models across various sectors (Warszawski et al., 2013, 2014). ISIMIP has recently completed its second phase, having more than 60 modelling groups contributing simulations to ISIMIP2a (reanalysis-driven hindcasts) and ISIMIP2b (bias-corrected GCM-driven historical and future scenarios). We present the JULES-ES configuration and experimental setup that has contributed to ISIMIP2b and will be the basis for further development in subsequent ISIMIP phases. An advantage of using JULES-ES as an offline impacts model is that it is computationally efficient compared to the closely aligned land surface scheme used in UKESM1 (Sellar et al., 2019), while using multi-model climate ensembles sample scientific uncertainty in land surface forcing that would not be possible within a single climate model framework.

This paper briefly describes the changes to JULES-GL7 (Wiltshire et al., 2020)

that form the JULES-ES configuration, the ISIMIP setup and an evaluation of the arising simulations. JULES-ES has been widely evaluated and applied for global biogeochemical modelling (Sellar et al., 2019; Slevin et al., 2017), including in the Global Carbon Budget (Friedlingstein et al., 2020). Here we focus on using JULES for impacts applications. Alongside this manuscript, we provide a suite to run JULES-ES following the ISIMIP2b modelling protocol (Frieler et al., 2017) for tailored impact projections that are consistent across sectors such as water and biomes. The suite includes the code to post-process output into ISIMIP formatted netcdf output and run the International Land Model Benchmarking (ILAMB) system to allow for quick evaluation (see Text S1). Data from the JULES-ES ISIMIP2b suite have been submitted to the biomes and water ISIMIP2b sectors and are available via the ISIMIP model archive (https://data.isimip.org/) and provide simulations of the historical and future land surface in the United Nations Environment Programme (2022) wildfire report. The JULES ISIMIP2b simulations with fire provide the basis for the contribution of JULES to the next FireMIP, which will use the ISIMIP3 set-up. The historical simulations and their evaluation are shown in section 3, with discussion and conclusions in Sections 4 and 5 respectively.

Materials and Methods

JULES-ES Configuration

To better represent variation in plant traits and managed land, we extend the standard representation of 5 Plant Functional Types (PFTs) in JULES-ES to 13, building on Harper et al. (2016), with 4 managed and 9 natural PFTs. Natural PFTs are extended by splitting trees into deciduous and evergreen types and then distinguishing between temperate and tropical broadleaf evergreen trees. These additional PFTs represent a wider range of leaf life spans and metabolic capacities. Evergreen trees typically have less access to nutrients, higher leaf mass per unit area, longer lifespans and low carbon assimilation and respiration rates, whereas a deciduous PFT typically has leaves with a higher nutrient concentration, shorter lifespan and lower leaf mass per unit area. Tropical broadleaf evergreen trees have lower maximum carbon assimilation rates than temperate trees. The 9 natural PFTs used are: tropical broadleaf evergreen trees (BET-Tr), temperate broadleaf evergreen trees (BET-Te), broadleaf deciduous trees (BDT), needle-leaf evergreen trees (NET), needle-leaf deciduous trees (NDT), C4 grasses, C4 grasses, evergreen shrubs (ESh), and deciduous shrubs (DSh). Harper et al. (2016) also updated several parameters required for calculating photosynthesis and respiration using the TRY database (Kattge et al., 2011). They also reduced the bias in model simulations by tuning parameters relating to leaf dark respiration, canopy radiation, canopy nitrogen, stomatal conductance, root depth, and temperature sensitivities of the maximum carboxylation rate of Rubisco (Vcmax) based on available observations. The 4 managed PFTs are C3 and C4 crop and pasture PFTs and are functionally similar to natu-

ral grasses but, in the case of crops are assumed not to be nitrogen limited and litter carbon is removed as a simple representation of crop harvest. Both crop and pasture surface types undergo land-use change according to externally forced time-varying land use. Within the respective crop/pasture fraction, only the C3 and C4 crop/pasture PFTs are allowed to grow, with the area of each determined by the TRIFFID dynamic vegetation module (Burton et al., 2019).

Outside of the managed land area, only the nine natural PFTs (including natural C3 and C4 grasses) can grow in the remainder of the grid box once the non-vegetated surfaces have been accounted for (urban, ice, lakes). As the prescribed crop or pasture fraction increases with land-use change, natural vegetation is removed from the portion of the grid box into which agriculture has expanded, representing anthropogenic land clearance. Conversely, when crop and pasture areas are reduced, the natural PFTs are allowed to recolonize the vacated grid box fraction. Bare soil occupies any remaining space once the vegetation dynamics have been simulated. Simple representations of fertilisation and harvesting are applied to the crop PFTs, but otherwise these are physiologically identical to the natural grasses. After accounting for land-use, the fractional coverage and biomass of each PFT within a grid box is determined by the TRIFFID dynamic vegetation model. Inter-PFT competition is based on vegetation height, with the taller vegetation shading and therefore dominating other PFTs (A. B. Harper et al., 2018).

The other major change introduced in JULES-ES is a representation of nitrogen and nutrient limitation effects on ecosystem carbon assimilation. The nitrogen component of JULES is described in Wiltshire et al. (2021). In brief, JULES-ES represents all the key terrestrial N processes. Inputs to the land surface are via biological fixation, fertilization and nitrogen deposition, with losses from the land surface occurring via leaching and gas loss, with Nitrogen deposition being externally provided to the model. JULES simulates a nitrogen-limited ecosystem by reducing the net primary productivity if there is insufficient available N to satisfy plant N demand. Any excess carbon is added to the plant respiration. The soil biogeochemistry is based on the representation of the four-pool RothC soil carbon model (Clark et al., 2011) consisting of decomposable plant material (DPM), resistant plant material (RPM), microbial biomass (BIO), and humus (HUM). For each soil carbon pool there is an equivalent soil nitrogen pool (Wiltshire et al., 2021). Nitrogen transfers between the organic and inorganic nitrogen pools depend on decomposition rates and the C to N ratio of the organic pool.

Another important change is the inclusion of a fire module. Fire is simulated in JULES by the fire model INFERNO (INteractive Fire and Emission algoRithm for Natural envirOnments; Mangeon et al. (2016)). Burned area is calculated from flammability and ignitions. Temperature, saturation vapour pressure, relative humidity, precipitation, together with soil moisture and fuel load from JULES give flammability by PFT, prescribed population density from HYDE3.2 (Goldewijk et al., 2017) gives human ignitions, and prescribed light-

ning from LIS/OTD version 2.3.2015 (Cecil, 2006) gives natural ignitions. Here we use INFERNO coupled to the dynamic vegetation model TRIFFID (Burton et al., 2019), enabling carbon cycle feedbacks from fire onto the land surface via vegetation mortality, regrowth, and burnt litter fluxes. Recent updates to INFERNO allow fire mortality to vary by PFT, and updates to the representation of land-use and PFTs in JULES allows for reduced burning in C3 and C4 crop PFTs (Burton et al., 2020), based on global trends of agricultural fire suppression (Andela et al., 2017; Bistinas et al., 2014).

Modifications for ISIMIP2b

In the ISIMIP JULES-ES configuration the TRIFFID period has been reduced from a 10-day to a 1-day period in order to allow a shorter restart periods necessary to meet the diagnostic requirements of ISIMIP (a large number of variables on short temporal scales). A daily TRIFFID period also allows the vegetation dynamics to respond more realistically to variations in plant productivity on shorter timescales, although the effect of this change is minimal in test historical runs.

Another key difference to the standard setup of JULES is the use of daily meteorological driving data. JULES needs a model timestep of no more than 1 hour to accurately simulate the diurnal cycle and exchange of heat, water and momentum and avoid numerical instabilities. In the ISIMIP experimental setup, we use the internal disaggregator (Williams & Clark, 2014) to calculate driving data values at the model timestep of 1 hour, based on the method used by the IMOGEN model (Huntingford et al., 2010). The diurnal cycle of downward shortwave radiation is calculated from the position of the sun in the sky. Temperature is calculated from a sinusoidal function with a maximum 0.15 of a daylength after local noon, normalised by the diurnal temperature range. Downward longwave radiation is a linear function of temperature, and specific humidity is kept below saturation at each timestep. Precipitation is considered to occur in a single event, with a globally specified 'duration' parameter (6h for convective rainfall, 1h for large-scale rainfall, convective snowfall and large-scale snowfall). Given that this event does not, by construction, overlap with midnight GMT, on average, this produces a spurious trapezoidal diurnal cycle, which is zero at midnight GMT (Williams & Clark, 2014). Precipitation above 350 mm/day is redistributed. Note that convective precipitation occurs only on a fraction of the grid box (Best et al., 2011), set to 30% in the ISMIP2b runs, and within this fraction is modelled as a negative exponential distribution (Johannes Dolman & Gregory, 1992). Therefore, the grid box average intensity is not the same as the effective intensity at a point. Given the strong effect of intensity on canopy interception and runoff, the water cycle in the model is sensitive to the duration parameter choices (Williams & Clark, 2014). See Figure S1 for plots showing that using the disaggregator has little effect on vegetation that we would expect to be influenced by rainfall.

ISIMIP2b protocol

The ISIMIP2b experiments focus on understanding different levels of mitigation. They are consistent with the international commitment made under the Paris Agreement to stabilise global warming at well below 2°C, relative to pre-industrial mean temperatures. ISIMIP2b uses simulations from the Coupled Model Inter-comparison Project 5 (CMIP5), using an historical scenario (1860-2006) and the RCP2.6 and RCP6.0 future concentration pathways (2006-2099) to represent a higher ambition, lower temperature outcome and a low ambition pathway respectively (Riahi et al., 2017). Land-use data and population density are based on the Shared Socioeconomic Pathway (SSP2) scenario and applied to RCP2.6 and RCP6.0 simulations. To capture a range of climate sensitivities, four CMIP5 GCM driving models are chosen: GFDL-ESM2M, HadGEM2-ES, IPSL-CM5A-LR and MiROC5. The GCM driving data is global bias-corrected daily data at 0.5° resolution (Hempel et al. (2013), Lange (2018) and Frieler et al. (2017)). The bias-correction methodology adjusts multi-year monthly mean distribution for the period 1979 to 2013, using CMIP5 RCP8.5 post-2006 (the end of CMIP5 "historic" period), such that trends and inter-annual variability are preserved in absolute and relative terms for temperature and non-negative variables respectively Lange (2018). Transfer functions are used to adjust the distributions of daily anomalies from monthly mean values. The ISIMIP2b bias correction includes humidity as well as shortwave and longwave radiation using quantile mapping. ISIMIP2b bias-correction methods adjust distributions independently for each variable, grid cell and month, preserving the statistical dependencies between variables, in space and changes over time. The bias correction approach preserves the trends (and therefore sensitivities) from different GCMs but removes absolute biases over the reference period. Each GCM therefore has a different variability and simulated climate outside of the reference period. Some small biases remain after bias-correction, particularly in precipitation (Figure S2), where biases are a small fraction of total local rainfall but can affect precipitation particularly in the South America (Figure S3). As part of the setup provided here, we include code for preparing JULES data for submitting to ISIMIP and ensuring it conforms to the strict protocols (see Text S1) and the ILAMB system for rapid evaluation of the simulations (see Text S2).

Model Evaluation

We evaluate the model for key impacts sectors, and use the International Land Model Benchmarking (ILAMB) tool (Collier et al., 2018) to assess model performance for GPP, ET, runoff and albedo. ILAMB evaluates performance against observations from remote sensing, reanalysis data and fluxnet site measurements and produces graphical and statistical scores of model results. We compare model GPP against the upscaled fluxnet product from Jung et al. (2011), ET against GLEAM (Miralles et al., 2011) and MODIS (Mu et al., 2011) estimates, runoff against Dai and Trenberth (2002), albedo against the GEWEX SRB radiation observations (Stackhouse et al., 2011) and burnt area against Global

Fire Emission Database version 4 with small fires (GFED4s; Van Der Werf et al. (2017). As ILAMB doesn't include vegetation cover evaluation, we also include the Manhattan Metric (Kelley et al., 2013) comparison against from ESA CCI Land Cover tree, shrub, wood and grass cover (Harper et al., 2022). Results and further details of the ILAMB and vegetation cover analysis are provided in Text S2. We evaluate the historical simulations separately for each GCM because the bias correction preserves inter-annual differences between GCMs. We conduct evaluation over common time periods between observations and simulation using the historic and, for observational periods beyond the end of 2006, RCP6.0.

The experimental suite

We provide a full setup for running the ISIMIP2b simulations using JULES-ES in the form of the suite u-cc669 available via the Met Office Science Repository Service (MOSRS - https://code.metoffice.gov.uk/trac/roses-u see data availability section for information). The bias corrected driving data is available from ISIMIP at https://www.isimip.org/gettingstarted/input-data-bias-adjustment/. We also use the following datasets from ISIMIP. Where preprocessing of these is required to use this data within JULES, this preprocessing code is also part of the suite.

- CO_2 concentration
- Future land-use patterns
- Nitrogen deposition
- Land-sea mask
- TRIP is used for river routing in JULES, therefore a TRIP 0.5° river routing ancillary is also required and available from http://hydro.iis.u-tokyo.ac.jp/~taikan/TRIPDATA/.

Model evaluation

Water

We evaluated the water cycle using runoff derived from Dai and Trenberth (2002) for the 50 largest river catchments. Estimated observed mean basin runoff combines river flow measurements at downstream gauge stations with a river flow model to estimate the flow at the river mouth. By assuming there are no losses from the river, we calculated the long-term mean, basin averaged runoff by dividing the river flow at the river mouth by the basin area.

Particularly in temperate regions north and south of the equator, simulations using all 4 sets of driving data show similar biases. However, differences between the driving datasets are greatest in tropical or sub-tropical river catchments

(Figure 1). This is particularly evident in the Amazon basin, where mean runoff biases range from approximately 0 in the simulation driven by HADGEM2-ES, to more than -0.6mm day^{-1} in the simulation driven by IPSL-CM5A-LR. Strong variations between the simulations are also seen in the Brahmaputra basin (Figure 2). The general underestimate of runoff in the higher latitudes may be due to the treatment of moisture infiltration into partially frozen soils (see below) but could also be caused by biases in precipitation estimates due to the gauge "under-catch" of snow (Adam & Lettenmaier, 2003). In arid and semi-arid basins river flow and runoff tends to be over-estimated, which could be due to anthropogenic water extraction which disproportionately affects groundwater depletion (Richey et al., 2015).

Figure 2 compares the long-term monthly mean river flow (1980-2014 inclusive where observations are available) over the six largest rivers to those of down-stream observations in Dai (2021). All the simulations reproduce the overall seasonal river flow over the Amazon. After the wet season, the modelled river flows decline earlier than observed and the simulated river flows at "low water" are too low. This could be due to too much evaporation in the drier months (see ET for JJA in Figure S4) and/or the simulated speed of flow through the soil and/or river channel being too fast. Though GFDL-ESM2M and IPSL-CM5A-LR driving precipitation data also has a dry bias during the dry season (Figure S3). All simulations over-estimate river flow over the Congo, mainly due to over-estimates in the rainy months. This could be driven by too little evaporation from the vegetation canopy or from flooded areas. The simulations reproduce the seasonal river flow over the Orinoco well. The timings of peak river flow for the Chiangjiang and Brahmaputra are well simulated although the amplitudes are too low. Dams, which we do not model, are likely to affect the observed seasonal cycle. The simulated river flow over the Mississippi lags observations by several months. This lag is also evident over many high latitude basins (not shown). The observed river flow peak is mainly driven by Spring melt, whereas the simulated river flow peak is in line with that of precipitation. This is due to this configuration allowing significant soil infiltration of snow melt when the soil surface is mainly frozen, rather than resulting in surface runoff. This also may result in the underestimate of annual river flow because once the water has infiltrated the soil it may then be evaporated.

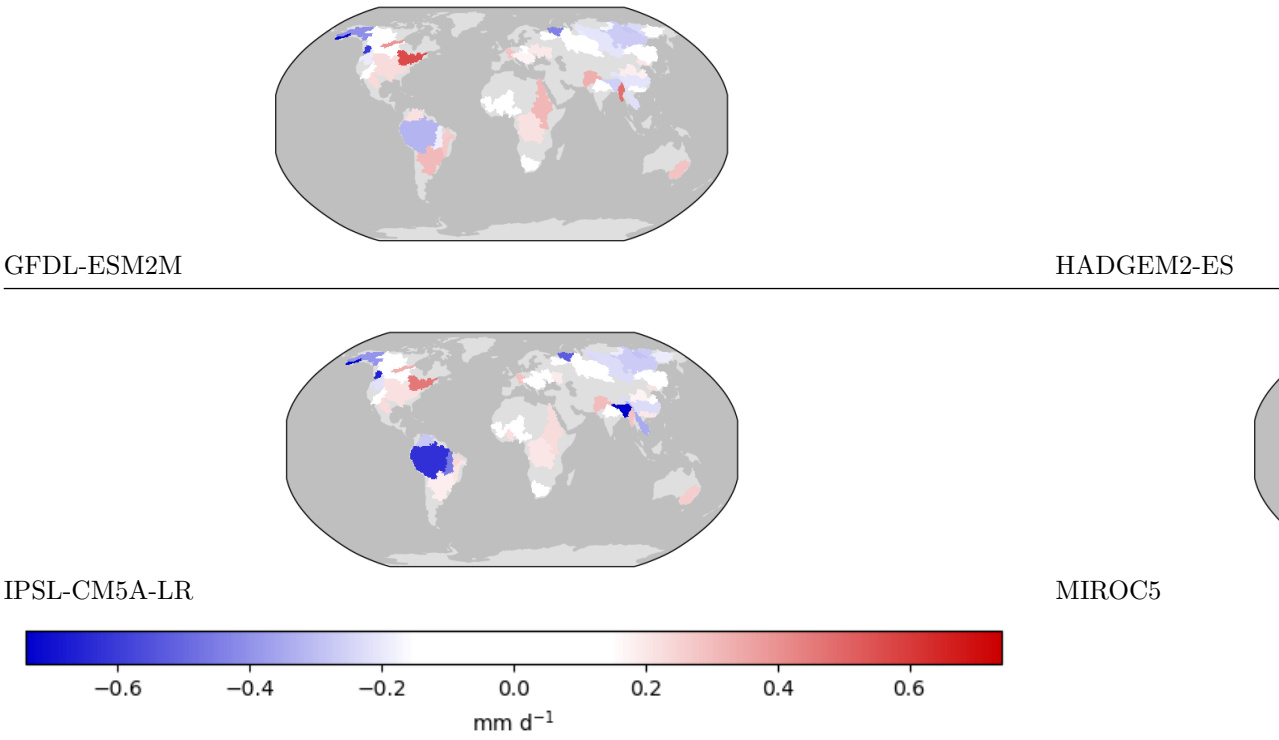

Figure 1 Multi-year mean bias of catchment scale runoff simulated by JULES driven by 4 sets of climate driving data compared to runoff derived from (Dai, 2021). Number of years of observations contributing to the multi-year mean varies depending on catchment, however, observations within the period 1980-2006 were accepted. ISIMIP2b forcing data derived from 4 CMIP5 GCMs: GFDL-ESM2M; HadGEM2-ES; IPSL-CM5A-LR; MIROC5.

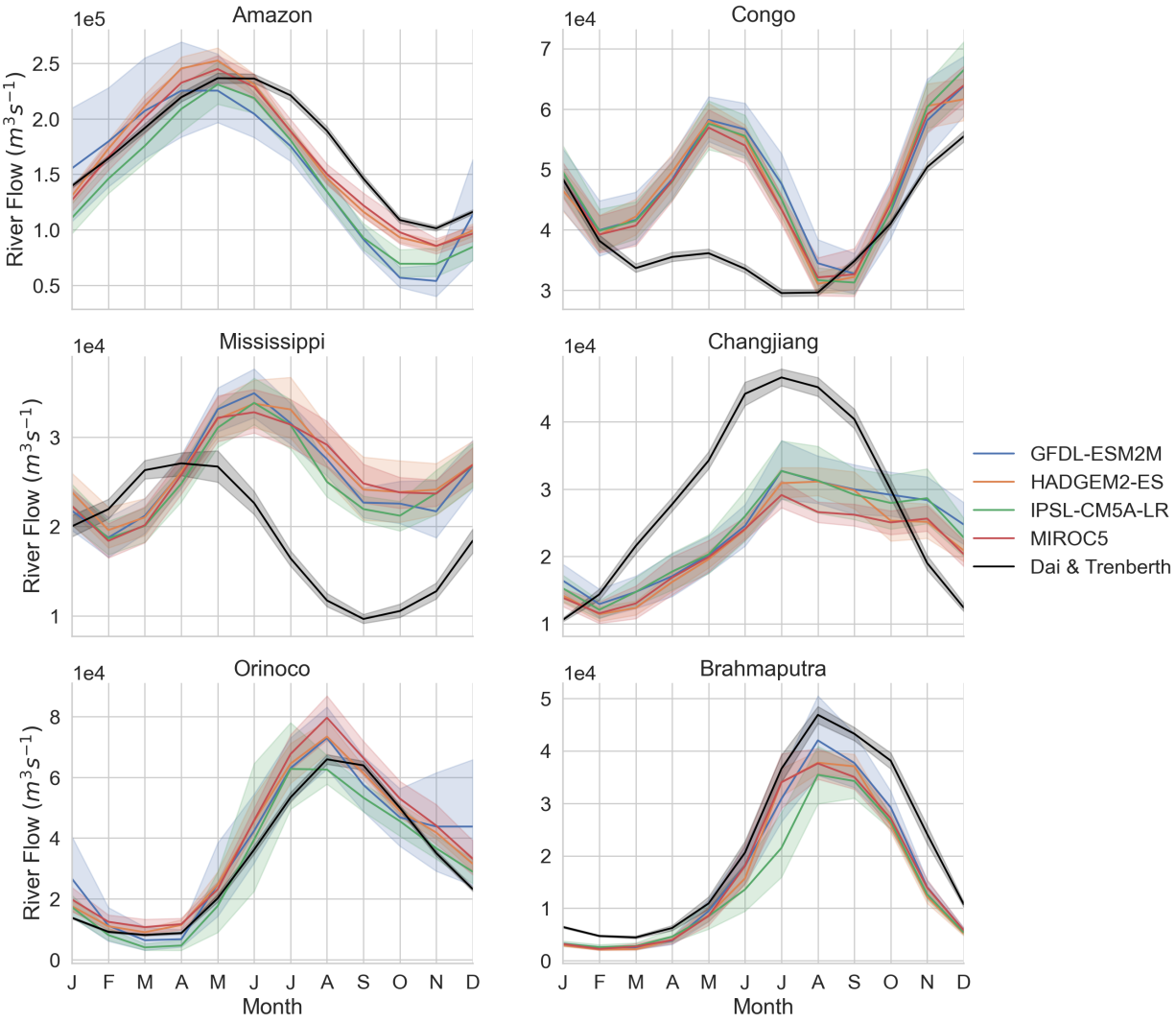

Figure 2 Comparison of the simulated long term monthly mean river flow with observations (Dai, 2021) for the six largest rivers: a) Amazon (Obidos, -1.95N,-55.51E); b) Congo (Kinshasa, -4.3N, 15.3E); c) Orinoco (Pte Angostu , 8.15N,-63.6E); d) Changjiang (Datong, 30.77N, 117.62E); e) Brahmaputra (Bahadurabad, 25.18N, 89.67E); f) Mississippi (Vicksburg 32.31N, -90.91E). The observations are over the time period 1980 to 2010.

Surface fluxes

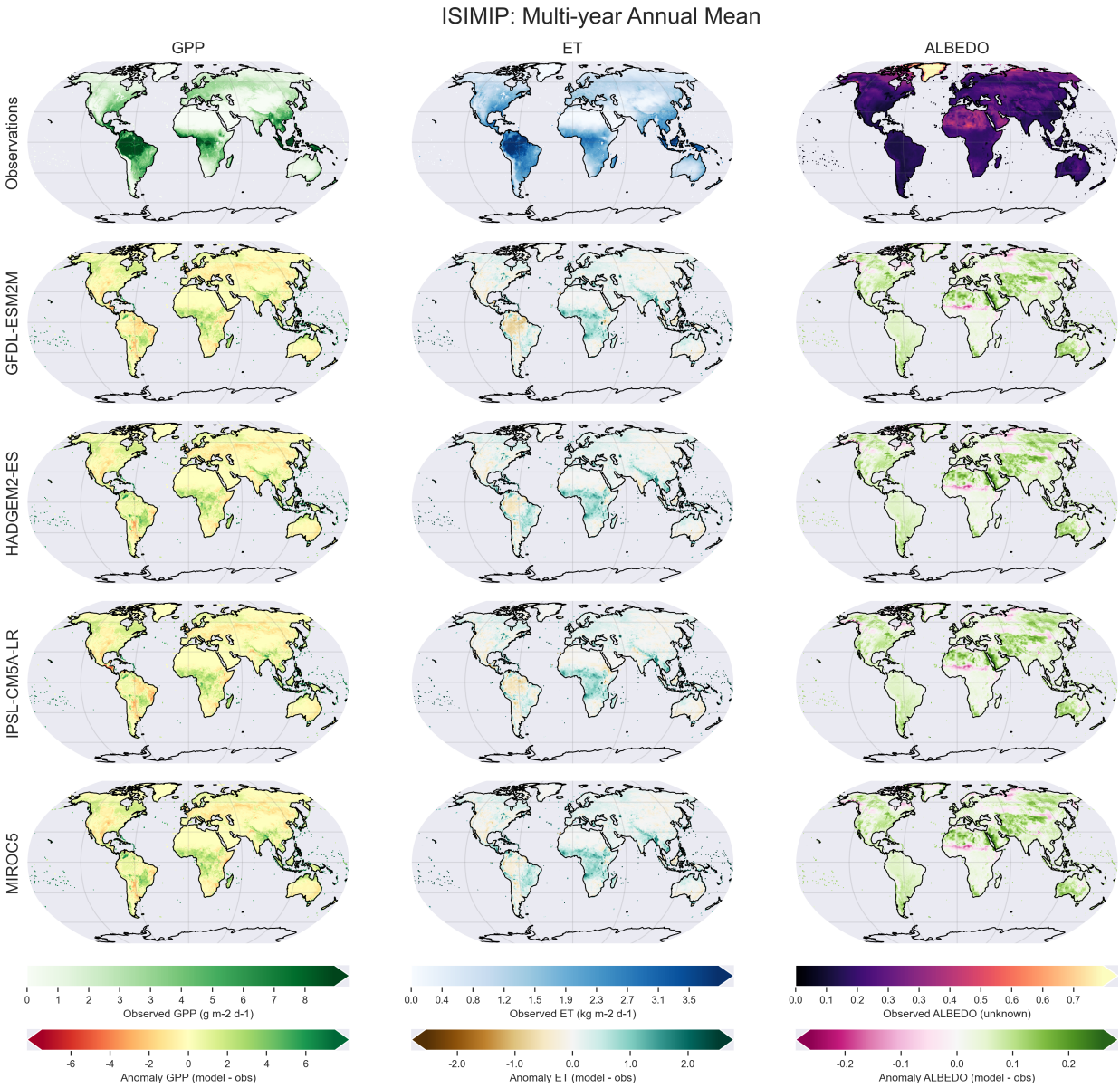

Figure 3 Multi-year annual mean for GPP (column 1), Evapotranspiration (Column 2) and Albedo (column 3) for observations (row 1) and subsequent rows show the anomaly compared with observations for each set of ISIMIP2b forcing data derived from: GFDL-ESM2M (row 2), HADGEM2-ES (row 3), IPSL-CM5A-LR (row 4) and MIROC5 (row 5). Observations are downloaded from iLAMB (https://www.ilamb.org/doc/ilamb_fetch.html) and the datsets shown

are GBAF for GPP (Jung et al., 2011), GLEAM for ET ((Miralles et al., 2011) and GEWEX.SRB for Albedo (Stackhouse et al., 2011).

Global Gross Primary Productivity (GPP) is 134-137 PgC/yr, depending on driving data, which is above the estimate off IPCC AR6 (Canadell et al., 2021) of 113 PgC yr-1, but agrees well with the estimates of 146 $\pm$ 21 PgC/yr of Cheng et al. (2017; Table S1). Net Biome Productivity (NBP) is 0.94-1.46 PgC/yr between 2011-2020, within the 1.0-2.8 PgC/yr range estimated by the Global Carbon Budget (Friedlingstein et al., 2022). All simulations show positive GPP biases in similar regions, such as central and southern Africa, south of the Himalaya and east towards Bangladesh and Myanmar compared to Jung et al. (2011) observations (Figure 3). South America is a more complicated picture with Brazil broadly split between negative GPP to the northeast and positive GPP to the country's southeast. For Brazil, the ET bias has a more northwest – southeast split, with the northwest having a slightly negative bias and the southeast more positive. The northwest bias in ET and the bias in GPP in South America is more prominent and wide-spread in early wet season (September-November) when driven by climate data from GFDL-ESM2M and IPSL-CM5A-LR (see Figure S4) and is due to a longer dry season in both sets of driving data (Figure S3), with rains starting in October rather than September. The far north of Columbia, Bolivia and Argentina also have a negative bias in both GPP and ET across the simulations. Australia also has a north-south split with a slight positive ET bias to the north and the inverse to the south.

Albedo (Figure 3 right column) generally shows a positive bias across most regions and simulations. However, there are small regions with a negative bias, for example, south of the Sahel and small regions at higher northern latitudes. Eastern Siberia has a positive bias in all simulations (see Discussion).

Biomes

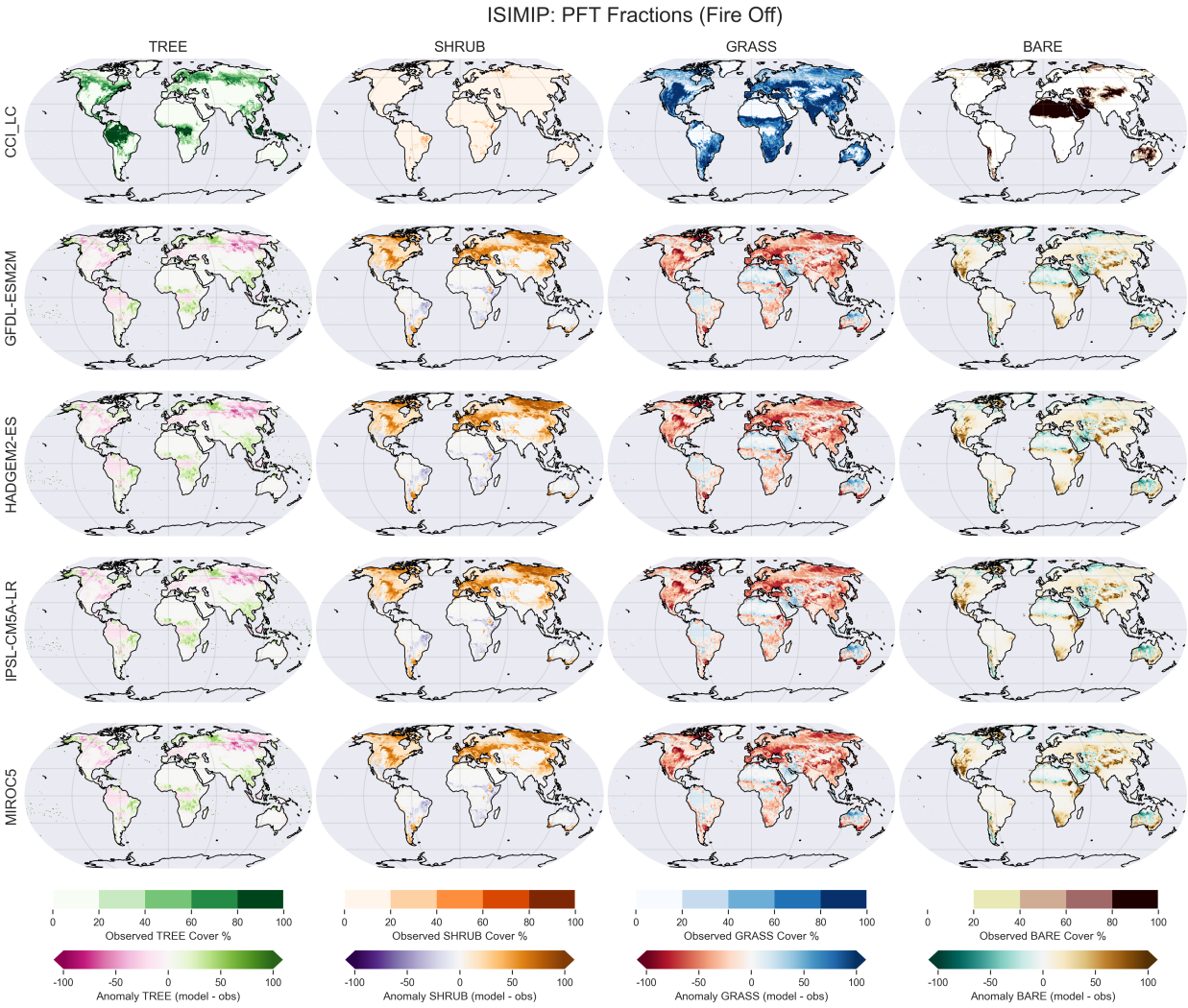

Figure 4 Observed vegetation fractional cover, derived from ESACCI Land Cover (v2.0.7) for 2010 (K. L. Harper et al., 2022), for (left to right) tree, shrub, grass and unvegetated (bare) fraction. Subsequent rows show the difference between model (without fire) and ES CCI observations for each set of driving data.

All simulations show similar vegetation cover patterns that largely follow observations, capturing high tree cover fractions in boreal and tropical forests, grass cover in tropical, temperate and boreal grasslands and bare ground in arid regions (Figure 4). There are, however, some biases common to all simulations. Tree cover fraction is too high globally, with a simulated range of

4.97-5.31Mkm^2 higher than observations depending on driving data (Table S2). In the observations, shrub and grasses dominate eastern Siberian Taiga in the model instead of tree cover. There is also slightly too much shrub cover in tropical forests at the expense of tree cover, contributing to a global bias of 1.22-1.31 Mkm^2. Conversely, simulated tropical tree cover is too high in savanna regions, giving the impression of more continuous and less fragmented forests across the tropics (Figure 4). Boundaries between temperate and warm temperate woodlands/forests and tropical forests are too sharp, suggesting JULES-ES does not capture processes in temperate woodland transition. Savanna and grasslands tend to be too narrow, with more bare soil in the models in semi-arid regions such as southern Africa, the Mojave desert and the Sahel.

Fire

Burnt area is similar across all four simulations (Figure 5). The model simulates present-day burnt area well compared to satellite observations, with the global total burnt area average for 2000-2020 observed by MODIS CCI v5.1 as 4.55 Mkm^2, and the model simulating between 3.94-4.43 Mkm^2 depending on driving data (Table S3). The model captures the high burnt area in southern hemisphere Africa - a common area of low bias in global fire models (Hantson et al., 2020). The model also performs better than other FireMIP models at simulating the high burnt areas in northern hemisphere Africa (Hantson et al., 2020), though fire is still lower than in observations. This is partly due to very low simulated burnt areas in Nigeria's Guinean savanna, which Kelley et al. (2019) show is likely inevitable in global parameterisations of population density and agricultural drivers of burnt area. Other regional biases include too high burnt area in South America and too low in Eurasia and northern Australia (Figure 5).

Fire is simulated well in savanna bands (15 degrees north and south), which improves the representation of tree cover by reducing the positive bias compared to observations (Figure 6; Table S2). The inclusion of interactive fire has the overall effect of decreasing simulated global tree cover (from 38.66-39, depending on driving data to 34.32-35.65 Mkm^2) to more in line with observations (34.86 Mkm^2) and increasing grasses and bare soil. In the tropics, this tends to bring the modelled "forest" (areas dominated by trees) more in line with the observations, with high simulated tree cover restricted to observed forested areas. However, including fire does reduce tree cover in Savanna areas (Figure S5), particularly in Africa, which diminishes performance in spatial distribution (Table S2). Fire reduces shrub cover to well below observations (Table S2), though given the well documented issues in distinguishing tall and short woody vegetation (Gerard et al., 2017), it is probably more meaningful to assess total woody cover. Here, including fire reduces model bias (from 6.19-6.59 to -3.60--2.25 Mkm^2) and improves the spatial pattern (Table S2). Including fire reduces the global bias of high GPP, bringing global total down by ~2 PgC/yr across all simulations (Table S1). However, fire does slightly degrade GPPs spatial pat-

tern (Table S1). Including fire also reduced global NBP (Table S1) by 0.12-0.38 PgC/yr, depending on driving data.

Fire alleviates some of the high bias in ET, improving the models' overall performance (Table S4). In semi-arid areas we already over-estimate river flow (in part probably due to human extraction). The addition of fire lowers ET, thereby increasing river flow bias in semi-arid regions, which slightly degrades overall runoff performance (Figure S6). Fire also improves spatial pattern of albedo (Table S5), though seasonal performance decreases. This is in line with well-documented biases in fire seasonal cycles across all global fire models (Hantson et al., 2016, 2020), including in previous JULES configurations incorporating INFERNO (Burton et al., 2019, 2022).

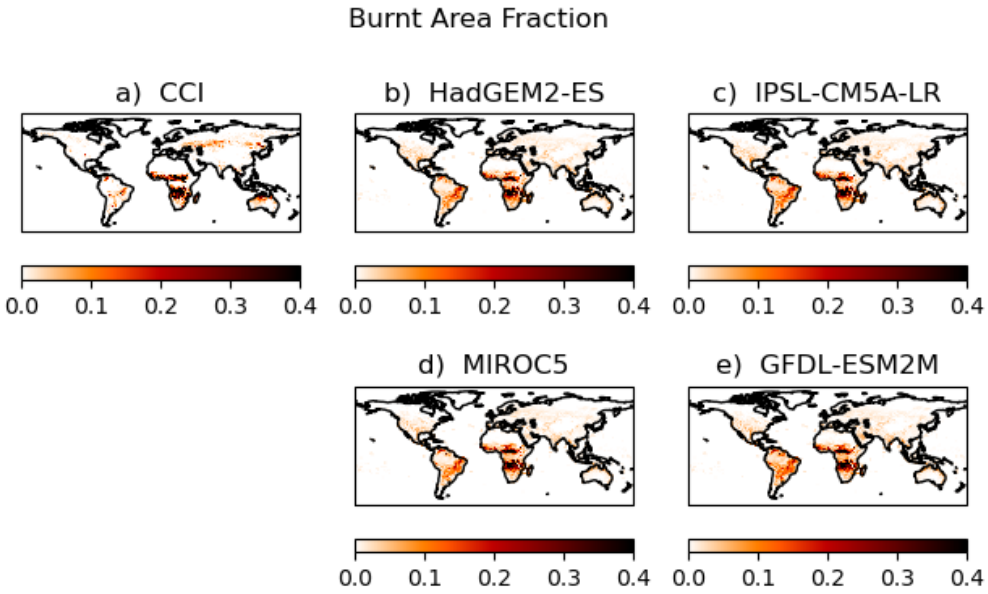

Figure 5 Present day burned area fraction (2000-2020) from and Fire CCI observations (a) and modelled by JULES driven by HadGEM2-ES (b), IPSL-CM5A-LR (c), MIROC5 (d), GFDL-ESM2M (e)

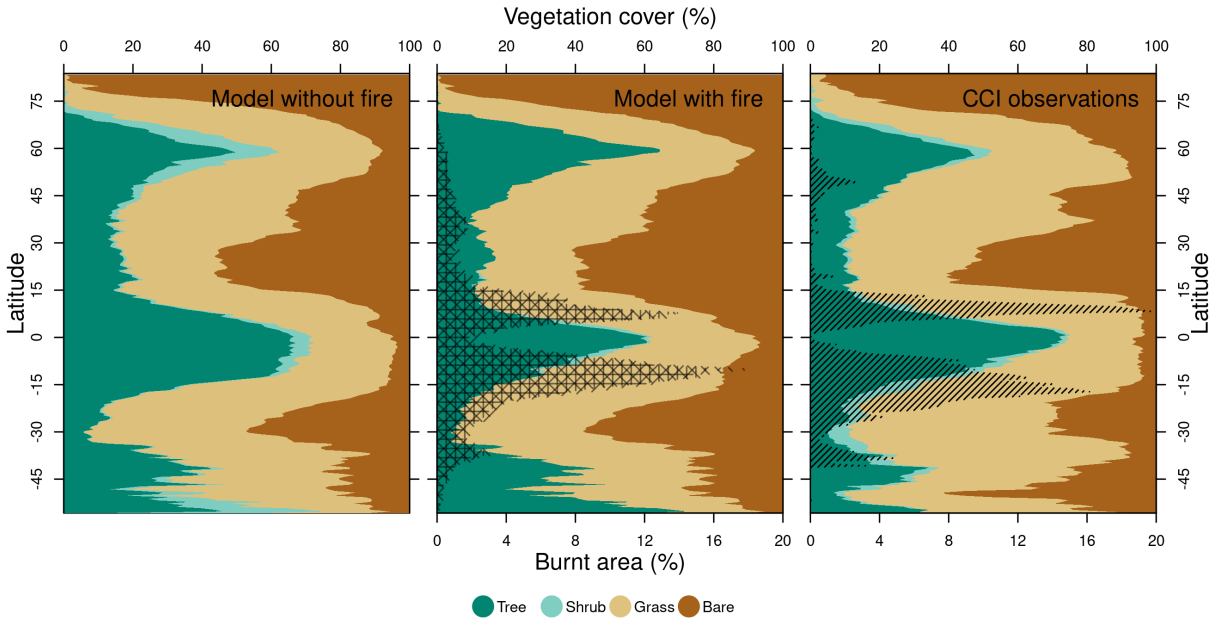

Figure 6 Modelled vegetation cover without fire (left) and with fire (middle) compared to observations from ESA CCI Land Cover and Fire (right). Dark green, light green, light brown, dark brown indicates tree, shrub, grass and unvegetated fraction of the latitude band. Black hashing indicates burnt area, with observations taken from MODIS CCI v5.1 (Chuvieco et al., 2018). In "Model with fire", burnt area from the 4 driving models is shown by hatching at 4 different angles.

Discussion

We have presented simulations of the JULES-ES land surface model, run according to the ISIMIP2b protocols using bias-corrected climate model data from 4 GCMs for the historical period. The configuration will be used to perform simulations under 2 future scenarios (RCP2.6 and RCP6.0). The JULES-ES ISIMIP2b configuration simulates the surface fluxes (GPP, ET, albedo) reasonably well. Including fire improves the ET and albedo, but not the GPP which is biased high. Including fire in the simulations currently degrades runoff (Table S6).

The configurations of JULES can capture the annual cycle of many of the largest rivers, although high latitude rivers and managed rivers are generally not captured as well. Including structural hydrological developments, such as dams and reservoirs, would likely improve the simulations of managed rivers. Pre-

viously, Falloon et al. (2011) found that GCM precipitation biases contribute to errors in TRIP river flows for some basins in both HadGEM1 and HadCM3. In this study, we use bias-corrected data which reduces these errors, meaning that differences in JULES-ES results between the driving models are due to differences in inter-seasonal or inter-annual variability between driving models (e.g. Figure S3). However, errors in evapotranspiration, runoff generation or other missing processes e.g., snow accumulation and snow melt processes, could also contribute. Uncertainty in precipitation due to the sparsity of observation networks and the under-catch of solid precipitation for high latitude (Falloon et al., 2011) and altitude rivers e.g., in the Himalaya (Mathison et al., 2015), means that it is difficult to interpret model performance in these basins.

Some basins show the same bias direction in runoff (Figure 1) and ET (Figure 3), notably that the Amazon is too dry for both variables and the Nile too wet, whereas we would expect opposing biases if they were from land surface simulation. In these basins, there is a dry and wet bias (respectively) in the driving precipitation data (Figure S2). HadGEM2-ES and IPSL-CM5A-LR have particularly dry driving data in the Amazon, and results in the driest runoff and ET in the simulation. This translates to biases in GPP (Figure 3) and vegetation cover (Figure 4). So, while ISIMP bias-correction reduces climate model biases compared to those in an Earth System Model (see evaluation in Sellar et al. (2019)) or when run with a none-bias corrected climate (Burton et al., 2022), they are not eliminated.

Land cover is an important factor for the surface fluxes. Grassy regions for example, correlate with the regions of positive ET bias. The annual mean global GPP biases are small, but this is not the case for GPP on a seasonal timescale and over a smaller region such as South America. The albedo and land cover area bias are also closely related. For example, the number of trees may lead to a higher or lower albedo. This is particularly important at high latitudes where there is snow cover, for example the positive albedo bias in Eastern Siberia is because JULES simulates too few trees and too much grass there. This positive bias in grass cover, affects the snowcover in these regions, which in turn affects the albedo. JULES represents the bending and partial burying of vegetation by snow (Ménard et al., 2014), however the settings controlling this interaction described in Sellar et al. (2019) have been tuned for the coupled UKESM1 model rather than the standalone JULES model. Eastern Siberia is a vulnerable region which has experienced increased climate-related impacts, including heatwaves (Ciavarella et al., 2021) and fires (Kelley et al., 2019); it is very likely that climate change will exacerbate these feedbacks by the end of the 21st century (United Nations Environment Programme, 2022). Developments by (Mercado et al., 2018) which improve the representation of plant acclimation to thermal stress may improve spatial variations across different vegetation types in JULES.

In general, the simulations with fire improve the vegetation distribution. Developing JULES to include these processes will improve simulations for these areas and properly capture the climate impacts there. The results show that there

are too few trees compared to observations for western parts of Brazil. The simulations with fire on improve tree cover in savanna, which is consistent with the findings of Lasslop et al. (2016) and Staver et al. (2011), however there is still ongoing discussion around how much impact fire really has on tree cover in the savanna compared to other dry disturbances such as wind throw, heat stress, rainfall distribution (Brovkin et al., 2009; Veenendaal et al., 2018).

Conclusions

We have presented a configuration of JULES-ES set up to run and generate output following the ISIMIP protocols. We provide a suite for running the simulations that includes driving data, ancillaries, postprocessing and first look evaluation (ILAMB) for any phase of ISIMIP. Outputs using this set up were submitted to the biomes and water ISIMIP2b sectors, and our evaluation helps inform any difference between JULES-ES and other models participating in ISIMIP2b. The suite also provides a starting point for further JULES-ES developments. We include a fire set up for running with INFERNO to include representation of fire in anticipation of ISIMIP3 which will include a Fire Sector. We show that including fire has an impact on model results and is important to include in simulations of climate impacts. Therefore, while documentation of the configuration without fire will be useful for anyone using previously submitted results, we recommend using the configuration with fire in future JULES-ES development. Future work using this configuration and new phases of ISIMIP will focus on using the full benefit and extent of the ISIMIP ensemble to enable more in-depth exploration of climate impacts together with the quantification of earth system uncertainties, co-benefits of mitigation and adaptation to climate change.

Acknowledgments

Work and its contributors were supported by the Newton Fund through the Met Office Climate Science for Service Partnership Brazil (CSSP Brazil) (CB, CM, AH, AW), the Met Office Climate Science for Service Partnership South Africa (CSSP South Africa) (AH and CM). CM, KW, AW, AH, AS, EB, ER, CJ and NG were supported by the Met Office Hadley Centre Climate Programme funded by BEIS and Defra. The contribution by DIK and RJE was supported by the UK Natural Environment Research Council through The UK Earth System Modelling Project (UKESM, grant no. NE/N017951/1). DIK was additional supported by UK Natural Environment Research Council as part of the NC-International programme (NE/X006247/1) and the European Union's Horizon 2020 research and innovation programme under Grant Agreement No 101003536 (ESM2025 - Earth System Models for the Future)

Open Research

The JULES-ES for ISIMIP configuration (based on JULES version 5.5) is preserved at https://code.metoffice.gov.uk/trac/roses-u/browser/b/k/8/8/6 (fire off) and https://code.metoffice.gov.uk/trac/roses-u/browser/c/f/1/3/7 (fire on). JULES and associated configurations are freely available for non-commercial research use as set out in the JULES user terms and conditions (http://jules-lsm.github.io/access_req/JULES_Licence.pdf). For a comprehensive guide on how to access, install and run the configurations used in this research, we direct the reader to Appendix A of Wiltshire et al. (2020) available at https://gmd.copernicus.org/articles/13/483/2020/#section6

The data and code used for the evaluation of the JULES-ES outputs with iLAMB in the study are available at https://www.ilamb.org/datasets.html and https://github.com/rubisco-sfa/ILAMB with a BSD 3-clause "New" license (https://github.com/rubisco-sfa/ILAMB/blob/master/LICENSE.rst)

The JULES model data output used in the model evaluation in the study are available at https://data.isimip.org/, using the search tag 'jules-es-55' https://data.isimip.org/search/query/jules-es-55/ with Creative Commons Attribution 4.0 International license (https://creativecommons.org/licenses/by/4.0/)

References

Adam, J. C., & Lettenmaier, D. P. (2003). Adjustment of global gridded precipitation for systematic bias. *Journal of Geophysical Research: Atmospheres*, *108*(D9), 4257. https://doi.org/10.1029/2002JD002499Andela, N., Morton, D. C., Giglio, L., Chen, Y., Werf, G. R. van der, Kasibhatla, P. S., et al. (2017). A human-driven decline in global burned area. *Science*. https://doi.org/10.1126/SCIENCE.AAL4108Best, M. J., Pryor, M., Clark, D. B., Rooney, G. G., Essery, R. . L. H., Ménard, C. B., et al. (2011). The Joint UK Land Environment Simulator (JULES), model description – Part 1: Energy and water fluxes. *Geoscientific Model Development*, *4*(3), 677–699. https://doi.org/10.5194/gmd-4-677-2011Bistinas, I., Harrison, S. P., Prentice, I. C., & Pereira, J. M. C. (2014). Causal relationships versus emergent patterns in the global controls of fire frequency. *Biogeosciences*, *11*(18), 5087–5101. https://doi.org/10.5194/BG-11-5087-2014Brovkin, V., Raddatz, T., Reick, C. H., Claussen, M., & Gayler, V. (2009). Global biogeophysical interactions between forest and climate. *Geophysical Research Letters*, *36*(7). https://doi.org/10.1029/2009GL037543Burton, C., Betts, R., Cardoso, M., Feldpausch, R. T., Harper, A., Jones, C. D., et al. (2019). Representation of fire, land-use change and vegetation dynamics in the Joint UK Land Environment Simulator vn4.9 (JULES). *Geoscientific Model Development*, *12*(1), 179–193. https://doi.org/10.5194/GMD-12-179-2019Burton, C., Betts, R. A., Jones, C. D., Feldpausch, T. R., Cardoso, M., & Anderson, L. O. (2020). El Niño Driven Changes in Global Fire 2015/16. *Frontiers in Earth Science*, *8*, 199. https://doi.org/10.3389/FEART.2020.00199/BIBTEXBurton, C., Kelley, D. I., Jones, C. D., Betts, R. A., Cardoso, M., & Anderson,

L. (2022). South American fires and their impacts on ecosystems increase with continued emissions. *Climate Resilience and Sustainability*, *1*(1), e8. https://doi.org/10.1002/CLI2.8Canadell, J. G., Monteiro, P. M. S., Costa, M. H., Cotrim da Cunha, L., Cox, P. M., Eliseev, A. V., et al. (2021). Global Carbon and other Biogeochemical Cycles and Feedbacks. In M.-D. V., P. Zhai, A. Pirani, S. L. Connors, C. Péan, S. Berger, et al. (Eds.), *Climate Change 2021: The Physical Science Basis. Contribution of Working Group I to the Sixth Assessment Report of the Intergovernmental Panel on Climate Change* (pp. 673–816). Cambridge University Press, Cambridge, United Kingdom and New York, NY, USA. https://doi.org/https://doi.org/10.1017/9781009157896.007Cecil, D. J. (2006). LIS/OTD 0.5 Degree High Resolution Monthly Climatology (HRMC) (No. [1995-2014]). NASA Global Hydrology Resource Center DAAC, Huntsville, Alabama, U.S.A. Retrieved from http://dx.doi.org/10.5067/LIS/LIS-OTD/DATA303Cheng, L., Zhang, L., Wang, Y. P., Canadell, J. G., Chiew, F. H. S., Beringer, J., et al. (2017). Recent increases in terrestrial carbon uptake at little cost to the water cycle. *Nature Communications 2017 8:1*, *8*(1), 1–10. https://doi.org/10.1038/s41467-017-00114-5Chuvieco, E., Lizundia-Loiola, J., Lucrecia Pettinari, M., Ramo, R., Padilla, M., Tansey, K., et al. (2018). Generation and analysis of a new global burned area product based on MODIS 250 m reflectance bands and thermal anomalies. *Earth System Science Data*, *10*(4), 2015–2031. https://doi.org/10.5194/essd-10-2015-2018Ciavarella, A., Cotterill, D., Stott, P., Kew, S., Philip, S., van Oldenborgh, G. J., et al. (2021). Prolonged Siberian heat of 2020 almost impossible without human influence. *Climatic Change*, *166*(1–2), 1–18. https://doi.org/10.1007/S10584-021-03052-W/TABLES/3Clark, D. B., Mercado, L. M., Sitch, S., Jones, C. D., Gedney, N., Best, M. J., et al. (2011). The Joint UK Land Environment Simulator (JULES), model description – Part 2: Carbon fluxes and vegetation dynamics. *Geoscientific Model Development*, *4*(3), 701–722. https://doi.org/10.5194/gmd-4-701-2011Collier, N., Hoffman, F. M., Lawrence, D. M., Keppel-Aleks, G., Koven, C. D., Riley, W. J., et al. (2018). The International Land Model Benchmarking (ILAMB) System: Design, Theory, and Implementation. *Journal of Advances in Modeling Earth Systems*, *10*(11), 2731–2754. https://doi.org/10.1029/2018MS001354Dai, A. (2021). Hydroclimatic trends during 1950–2018 over global land. *Climate Dynamics*, *56*(11–12), 4027–4049. https://doi.org/10.1007/S00382-021-05684-1/FIGURES/14Dai, A., & Trenberth, K. E. (2002). Estimates of Freshwater Discharge from Continents: Latitudinal and Seasonal Variations. *Journal of Hydrometeorology*, *3*(6), 660–687. Retrieved from www.R-ArcticNET.sr.unh.eduFalloon, P., Betts, R., Wiltshire, A., Dankers, R., Mathison, C., Mcneall, D., et al. (2011). Validation of River Flows in HadGEM1 and HadCM3 with the TRIP River Flow Model. *Journal of Hydrometeorology*, *12*(6), 1157–1180. https://doi.org/10.1175/2011JHM1388.1Friedlingstein, P., O'Sullivan, M., Jones, M. W., Andrew, R. M., Hauck, J., Olsen, A., et al. (2020). Global Carbon Budget 2020. *Earth System Science Data*, *12*(4), 3269–3340. https://doi.org/10.5194/ESSD-12-3269-2020Friedlingstein, P., Jones, M. W., O'Sullivan, M., Andrew, R. M., Bakker, D. C. E., Hauck, J., et al. (2022).

Global Carbon Budget 2021. *Earth System Science Data*, *14*(4), 1917–2005. https://doi.org/10.5194/ESSD-14-1917-2022Frieler, K., Lange, S., Piontek, F., Reyer, C. P. O., Schewe, J., Warszawski, L., et al. (2017). Assessing the impacts of 1.5°C global warming - Simulation protocol of the Inter-Sectoral Impact Model Intercomparison Project (ISIMIP2b). *Geoscientific Model Development*, *10*(12), 4321–4345. https://doi.org/10.5194/GMD-10-4321-2017Gerard, F., Hooftman, D., van Langevelde, F., Veenendaal, E., White, S. M., & Lloyd, J. (2017). MODIS VCF should not be used to detect discontinuities in tree cover due to binning bias. A comment on Hanan et al. (2014) and Staver and Hansen (2015). *Global Ecology and Biogeography*, *26*(7), 854–859. https://doi.org/10.1111/GEB.12592Goldewijk, K. K., Beusen, A., Doelman, J., & Stehfest, E. (2017). Anthropogenic land use estimates for the Holocene - HYDE 3.2. *Earth System Science Data*, *9*(2), 927–953. https://doi.org/10.5194/ESSD-9-927-2017Hantson, S., Arneth, A., Harrison, S. P., Kelley, D. I., Colin Prentice, I., Rabin, S. S., et al. (2016). The status and challenge of global fire modelling. *Biogeosciences*, *13*(11), 3359–3375. https://doi.org/10.5194/BG-13-3359-2016Hantson, S., Kelley, D. I., Arneth, A., Harrison, S. P., Archibald, S., Bachelet, D., et al. (2020). Quantitative assessment of fire and vegetation properties in simulations with fire-enabled vegetation models from the Fire Model Intercomparison Project. *Geoscientific Model Development*, *13*(7), 3299–3318. https://doi.org/10.5194/GMD-13-3299-2020Harper, A. B., Cox, P. M., Friedlingstein, P., Wiltshire, A. J., Jones, C. D., Sitch, S., et al. (2016). Improved representation of plant functional types and physiology in the Joint UK Land Environment Simulator (JULES v4.2) using plant trait information. *Geoscientific Model Development*, *9*(7), 2415–2440. https://doi.org/10.5194/gmd-9-2415-2016Harper, A. B., Wiltshire, A. J., Cox, P. M., Friedlingstein, P., Jones, C. D., Mercado, L. M., et al. (2018). Vegetation distribution and terrestrial carbon cycle in a carbon cycle configuration of JULES4.6 with new plant functional types. *Geoscientific Model Development*, *11*(7), 2857–2873. https://doi.org/10.5194/GMD-11-2857-2018Harper, K. L., Lamarche, C., Hartley, A., Peylin, P., Ottlé, C., Bastrikov, V., et al. (2022). A 29-year time series of annual 300-metre resolution plant functional type maps for climate models. *Earth System Science Data Discussions*, *Submitted*.Hempel, S., Frieler, K., Warszawski, L., Schewe, J., & Piontek, F. (2013). A trend-preserving bias correction: The ISI-MIP approach. *Earth System Dynamics*, *4*(2), 219–236. https://doi.org/10.5194/ESD-4-219-2013Huntingford, C., Booth, B. B. B., Sitch, S., Gedney, N., Lowe, J. A., Liddicoat, S. K., et al. (2010). IMOGEN: An intermediate complexity model to evaluate terrestrial impacts of a changing climate. *Geoscientific Model Development*, *3*(2), 679–687. https://doi.org/10.5194/GMD-3-679-2010Johannes Dolman, A., & Gregory, D. (1992). The Parametrization of Rainfall Interception In GCMs. *Quarterly Journal of the Royal Meteorological Society*, *118*(505), 455–467. https://doi.org/10.1002/QJ.49711850504Jung, M., Reichstein, M., Margolis, H. a., Cescatti, A., Richardson, A. D., Arain, M. A., et al. (2011). Global patterns of land-atmosphere fluxes of carbon dioxide, latent heat, and sensible heat derived from eddy covariance,

satellite, and meteorological observations. *Journal of Geophysical Research*, *116*, G00J07. https://doi.org/10.1029/2010JG001566Kattge, J., Díaz, S., Lavorel, S., Prentice, I. C., Leadley, P., Bönisch, G., et al. (2011). TRY - a global database of plant traits. *Global Change Biology*, *17*(9), 2905–2935. https://doi.org/10.1111/j.1365-2486.2011.02451.xKelley, D. I., Prentice, I. C., Harrison, S. P., Wang, H., Simard, M., Fisher, J. B., & Willis, K. O. (2013). A comprehensive benchmarking system for evaluating global vegetation models. *Biogeosciences*, *10*(5), 3313–3340. https://doi.org/10.5194/BG-10-3313-2013Kelley, D. I., Bistinas, I., Whitley, R., Burton, C., Marthews, T. R., & Dong, N. (2019). How contemporary bioclimatic and human controls change global fire regimes. *Nature Climate Change 2019 9:9*, *9*(9), 690–696. https://doi.org/10.1038/s41558-019-0540-7Lange, S. (2018). Bias correction of surface downwelling longwave and shortwave radiation for the EWEMBI dataset. *Earth System Dynamics*, *9*(2), 627–645. https://doi.org/10.5194/ESD-9-627-2018Lasslop, G., Brovkin, V., Reick, C. H., Bathiany, S., & Kloster, S. (2016). Multiple stable states of tree cover in a global land surface model due to a fire-vegetation feedback. *Geophysical Research Letters*, *43*(12), 6324–6331. https://doi.org/10.1002/2016GL069365Mangeon, S., Voulgarakis, A., Gilham, R., Harper, A., Sitch, S., & Folberth, G. (2016). INFERNO: A fire and emissions scheme for the UK Met Office's Unified Model. *Geoscientific Model Development*, *9*(8), 2685–2700. https://doi.org/10.5194/GMD-9-2685-2016Mathison, C., Wiltshire, A. J., Falloon, P., & Challinor, A. J. (2015). South Asia river-flow projections and their implications for water resources. *Hydrology and Earth System Sciences*, *19*(12), 4783–4810. https://doi.org/10.5194/HESS-19-4783-2015Ménard, C. B., Essery, R., Pomeroy, J., Marsh, P., & Clark, D. B. (2014). A shrub bending model to calculate the albedo of shrub-tundra. *Hydrological Processes*, *28*(2), 341–351. https://doi.org/10.1002/HYP.9582Mercado, L. M., Medlyn, B. E., Huntingford, C., Oliver, R. J., Clark, D. B., Sitch, S., et al. (2018). Large sensitivity in land carbon storage due to geographical and temporal variation in the thermal response of photosynthetic capacity. *New Phytologist*, *218*(4), 1462–1477. https://doi.org/10.1111/NPH.15100Miralles, D. G., De Jeu, R. A. M., Gash, J. H., Holmes, T. R. H., & Dolman, A. J. (2011). Magnitude and variability of land evaporation and its components at the global scale. *Hydrology and Earth System Sciences*, *15*(3), 967–981. https://doi.org/10.5194/HESS-15-967-2011Mu, Q., Zhao, M., & Running, S. W. (2011). Improvements to a MODIS global terrestrial evapotranspiration algorithm. *Remote Sensing of Environment*, *115*(8), 1781–1800. https://doi.org/10.1016/j.rse.2011.02.019Riahi, K., van Vuuren, D. P., Kriegler, E., Edmonds, J., O'Neill, B. C., Fujimori, S., et al. (2017). The Shared Socioeconomic Pathways and their energy, land use, and greenhouse gas emissions implications: An overview. *Global Environmental Change*, *42*, 153–168. https://doi.org/10.1016/j.gloenvcha.2016.05.009Richey, A. S., Thomas, B. F., Lo, M. H., Reager, J. T., Famiglietti, J. S., Voss, K., et al. (2015). Quantifying renewable groundwater stress with GRACE. *Water Resources Research*, *51*(7), 5217–5238. https://doi.org/10.1002/2015WR017349Sellar, A. A., Jones, C. G., Mulcahy, J. P., Tang, Y., Yool, A., Wiltshire, A., et

al. (2019). UKESM1: Description and Evaluation of the U.K. Earth System Model. *Journal of Advances in Modeling Earth Systems*, *11*(12), 4513–4558. https://doi.org/10.1029/2019MS001739Slevin, D., Tett, S. F. B., Exbrayat, J.-F., Bloom, A. A., & Williams, M. (2017). Global evaluation of gross primary productivity in the JULES land surface model v3.4.1. *Geoscientific Model Development*, *10*(7), 2651–2670. https://doi.org/10.5194/gmd-10-2651-2017Stackhouse, P. W. J., Gupta, S. K., Cox, S. J., Mikovitz, J. C., Zhang, T., & Hinkelman, L. M. (2011). The NASA/GEWEX Surface Radiation Budget Release 3.0: 24.5-Year Dataset. *GEWEX News*, *21*(1).Staver, A. C., Archibald, S., & Levin, S. A. (2011). The global extent and determinants of savanna and forest as alternative biome states. *Science*, *334*(6053), 230–232. https://doi.org/10.1126/SCIENCE.1210465/SUPPL_FILE/STAVERSOM.REVISION.1.PDFUnited Nations Environment Programme. (2022). *Spreading like wildfire - The rising threat of extraordinary landscape fires*. Nairobi. Retrieved from https://wedocs.unep.org/bitstream/handle/20.500.11822/38372/wildfire_RRA.pdfVeenendaal, E. M., Torello-Raventos, M., Miranda, H. S., Sato, N. M., Oliveras, I., van Langevelde, F., et al. (2018). On the relationship between fire regime and vegetation structure in the tropics. *New Phytologist*, *218*(1), 153–166. https://doi.org/10.1111/NPH.14940Warszawski, L., Friend, A., Ostberg, S., Frieler, K., Lucht, W., Schaphoff, S., et al. (2013). A multi-model analysis of risk of ecosystem shifts under climate change. *Environmental Research Letters*, *8*(4), 044018. https://doi.org/10.1088/1748-9326/8/4/044018Warszawski, L., Frieler, K., Huber, V., Piontek, F., Serdeczny, O., & Schewe, J. (2014). The Inter-Sectoral Impact Model Intercomparison Project (ISI–MIP): Project framework. *Proceedings of the National Academy of Sciences*, *111*(9), 3228–3232. https://doi.org/10.1073/PNAS.1312330110Van Der Werf, G. R., Randerson, J. T., Giglio, L., Van Leeuwen, T. T., Chen, Y., Rogers, B. M., et al. (2017). Global fire emissions estimates during 1997-2016. *Earth System Science Data*, *9*(2), 697–720. https://doi.org/10.5194/ESSD-9-697-2017Williams, K., & Clark, D. B. (2014). Disaggregation of daily data in JULES. *Hadley Centre Technical Note*, *96*. Retrieved from https://library.metoffice.gov.uk/Portal/DownloadImageFile.ashx?fieldValueId=876Wiltshire, A. J., Duran Rojas, M. C., Edwards, J. M., Gedney, N., Harper, A. B., Hartley, A. J., et al. (2020). JULES-GL7: the Global Land configuration of the Joint UK Land Environment Simulator version 7.0 and 7.2. *Geoscientific Model Development*, *13*(2), 483–505. https://doi.org/10.5194/gmd-13-483-2020Wiltshire, A. J., Burke, E. J., Chadburn, S. E., Jones, C. D., Cox, P. M., Davies-Barnard, T., et al. (2021). Jules-cn: A coupled terrestrial carbon-nitrogen scheme (jules vn5.1). *Geoscientific Model Development*, *14*(4), 2161–2186. https://doi.org/10.5194/GMD-14-2161-2021